catalysts

MDPI

Communication

Dual-Modified Cu_2S with MoS_2 and Reduced Graphene Oxides as Efficient Photocatalysts for H_2 Evolution Reaction

Enna Ha [1,*,†], Zongyuan Xin [2,†], Danyang Li [1], Jingge Zhang [1], Tao Ji [1], Xin Hu [1], Luyang Wang [3] and Junqing Hu [1]

1 College of Health Science and Environmental Engineering, Shenzhen Technology University, Shenzhen 518118, China; 2150416001@stumail.sztu.edu.cn (D.L.); 2060411018@email.szu.edu.cn (J.Z.); jitao@sztu.edu.cn (T.J.); huxin@sztu.edu.cn (X.H.); hujunqing@sztu.edu.cn (J.H.)
2 Department of Applied Biology and Chemical Technology and the State Key Laboratory of Chirosciences, The Hong Kong Polytechnic University, Hung Hom, Kowloon, Hong Kong 999077, China; dongwan.xin@connect.polyu.hk
3 College of New Materials and New Energies, Shenzhen Technology University, Shenzhen 518118, China; wangluyang@sztu.edu.cn
* Correspondence: haenna@sztu.edu.cn
† These authors contributed equally to this work.

Abstract: Noble metal-free cocatalysts have drawn great interest in accelerating the catalytic reactions of metal chalcogenide semiconductor photocatalyst. In particular, great efforts have been made on modifying a semiconductor with dual cocatalysts, which show synergistic effect of a fast transfer of exciton and energy simultaneously. Herein, we report the dual-modified Cu_2S with MoS_2 and reduced graphene oxides (Cu_2S-MoS_2/rGO). The in situ growth of Cu_2S nanoparticles in the presence of MoS_2/rGO resulted in high density of nanoscale interfacial contacts among Cu_2S nanoparticles, MoS_2, and rGO, which is beneficial for reducing the photogenerated electrons' and holes' recombination. The Cu_2S-MoS_2/rGO system also demonstrated stable photocatalytic activity for H_2 evolution reaction for the long term.

Keywords: photocatalytic H_2 generation; Cu_2S-MoS_2/rGO heterostructure; interfacial contact; photostability

Citation: Ha, E.; Xin, Z.; Li, D.; Zhang, J.; Ji, T.; Hu, X.; Wang, L.; Hu, J. Dual-Modified Cu_2S with MoS_2 and Reduced Graphene Oxides as Efficient Photocatalysts for H_2 Evolution Reaction. *Catalysts* **2021**, *11*, 1278. https://doi.org/10.3390/catal11111278

Academic Editor: Vincenzo Vaiano

Received: 27 September 2021
Accepted: 20 October 2021
Published: 22 October 2021

1. Introduction

Chalcocite copper(I) sulfide (Cu_2S) is a typical p-type semiconductor with a bulk band gap of 1.2 eV [1], which has been extensively studied and used in many applications, such as cancer therapy [2,3], batteries [4], solar cell [5], catalyst [6], etc. Many efforts have been focused on the synthesis of Cu_2S nanostructures with different morphologies, sphere [7–9], nanowires [10,11], nanorods [12,13], nanosheets [14], and nanoplates [15,16]. In addition to its low cost, high earth abundancy, and low-toxicity, Cu_2S is nearly ideal to capture and convert sunlight into useful chemical fuel. The conduction band (CB) of Cu_2S is more negative than the proton reduction potential, and the narrow band gap enables the absorption of solar energy in the visible regime [17]. However, the issue remains its poor photocatalytic activity due to a rapid exciton recombination. Although much effort has been made to synthesize the Cu_2S of various nanostructures, a systematic study on the morphology–performance relationship and the suppression of photoelectron recombination remain the key challenges to improve their photocatalytic performances.

Formation of heterogeneous structures is a key approach for improving the activity of photocatalysts by suppressing the recombination probability of photoexcited electron-hole pairs [18,19]. One popular way is to decorate or incorporate photocatalysts with noble metal nanoparticles, such as platinum (Pt) or gold (Au), in order to shuttle the electrons from photocatalysts to the metal, as well as to provide more active sites for the redox reaction. However, the high cost and low availability of noble metals limit their industrial application. Molybdenum disulfide (MoS_2), graphene, and their hybrids were reported

to be promising two-dimensional nanomaterials that can replace Pt as a co-catalyst in the photocatalytic H_2 evolution reaction (HER) [20,21]. For instance, the formation of 2H phase MoS_2 nanosheets on novel Cu_2S snowflakes greatly enhanced the photocatalytic degradation of methyl orange [22]. A CuS@defect-rich MoS_2 core-shell structure exhibits good electrocatalytic hydrogen generation performance [23]. Our previous studies on the Cu_2ZnSnS_4 (CZTS)-MoS_2/rGO heterostructure also confirmed its better photocatalytic performance in hydrogen generation compared to noble metal-decorated CZTS [24].

On the other hand, 1T phase MoS_2, although not an intrinsically active semiconductor to capture light in photocatalytic reaction, showed good metallic properties and dense active sites compared to the traditional 2H phase [25]. By coupling 1T MoS_2 and Cu_2S through the rGO network, we expect pronounced enhancements in photocatalytic performance of Cu_2S, which has previously been inferior to many other systems. Herein, we synthesized the Cu_2S-MoS_2/rGO composites through a simple wet chemistry approach. We also systematically investigated the morphology effects on photocatalytic HER performance of Cu_2S nanostructures. The spherical Cu_2S nanoparticles anchored on MoS_2/rGO showed the highest photocatalytic hydrogen production rate with excellent long-term photostability, which surpasses those of many noble metal-modified semiconductors reported in the literature.

2. Results and Discussion

Figure 1a–e displays the typical transmission electron microscopic (TEM) images of as-synthesized Cu_2S, graphene oxide, MoS_2, MoS_2/rGO hybrids and Cu_2S-MoS_2/rGO composites. Cu_2S nanoparticles were grown on the MoS_2/rGO hybrid nanosheet to form a heterojunction structure. The Cu_2S nanoparticles are uniformly grown in a spherical shape with an average particle size of 8.7 ± 2.5 nm. The MoS_2 displays a multilayered structure with good contact with graphene oxide. High-resolution TEM images of Cu_2S-MoS_2/rGO heterostructure, shown in Figure 1f, clearly reveal the lattice fringes of a hexagonal Cu_2S (110) plane with d-spacing of 0.20 nm, which indicates their high degree of crystallinity and nanoscale interfacial contact. A 1T-MoS_2 (002) plane with d-spacing of 0.95 nm was also observed. In the preparation progress, ammonium diethyldithiocarbamate and dodecanthiol bind to the defective sites and exposed metal cations of MoS_2-rGO through polar covalent bond, where the Cu_2S can be in situ nucleated at a high temperature. Elemental analysis taken by EDS (Figure S1) shows a close stoichiometric number of Cu:S = 2:1 and Mo:S = 1:2.

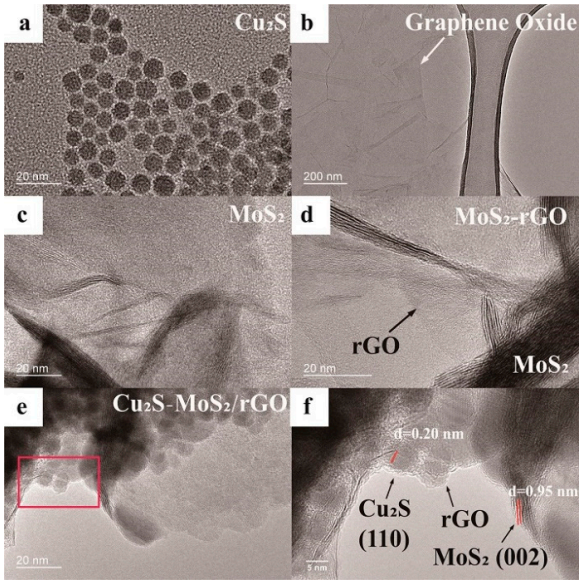

Figure 1. TEM images of (**a**) Cu_2S, (**b**) graphene oxide, (**c**) MoS_2, (**d**) MoS_2/rGO, (**e**) Cu_2S-MoS_2/rGO, and (**f**) high-resolution TEM images of Cu_2S-MoS_2/rGO composites.

The X-ray powder diffraction (XRD) patterns of the as-prepared Cu_2S-MoS_2/rGO composites, Cu_2S nanoparticles alone, and MoS_2/rGO hybrid are compared in Figure 2. For Cu_2S spherical nanoparticles, the characteristic peaks were observed at 37.4°, 45.8°, 48.5°, and 53.7°, which were well matched with the hexagonal chalcocite Cu_2S (JCPDS No. 026-1116). Peak broadening was observed since the crystallites are nano-sized. The as-prepared MoS_2/rGO showed the characteristic (002) peak of 1T MoS_2 at around 9° with d-spacing of 0.95 nm. For MoS_2/rGO, a second-order diffraction peak appeared at 18°, which could be assigned to a new (004) crystal plane. The corresponding d spacing difference between the two (002) peaks was around 0.33 nm, which is consistent with the hydrogen-bonding diameter (≈0.35 nm) of the ammonium ions in metal disulfides [18]. Cu_2S-MoS_2/rGO composites showed the pure phase of hexagonal Cu_2S (JCPDS No. 026-1116) without any side products. The peaks for 1T MoS_2 were not obvious in the composites, possibly due to the low loading amount of 1T MoS_2 (8.7 wt%) in the composites. This phenomenon has also been reported in other systems (ZnS-MoS_2/rGO and CZTS-MoS_2/rGO) [24,26].

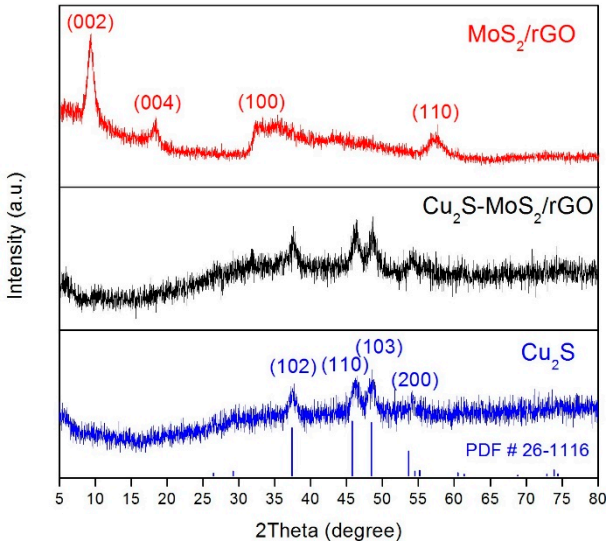

Figure 2. Powder XRD patterns of as-synthesized MoS_2/rGO, Cu_2S, and Cu_2S-MoS_2/rGO composites.

X-ray photoelectron spectroscopy (XPS) analyses were performed to investigate the chemical states and surface status of Cu_2S-MoS_2/rGO composites. The wide scan XPS spectrum, shown in Figure 3a, confirmed the coexistence of Cu, S, Mo, and C elements in the Cu_2S-MoS_2/rGO heterostructure. In the high-resolution XPS spectrum, Cu_2S-MoS_2/rGO showed a major C 1s signal from C-C at 284.9 eV and a tiny shoulder for C-O peak at 286.1 eV (Figure 3b,c), which identified the reduction of the O=C–O and C O bonds in graphene oxide and the formation of a good electron transfer network during the hydrothermal synthesis of MoS_2/rGO hybrid followed by further annealing for the growth of Cu_2S [25,27,28]. Two peaks observed at 932.2 and 952 eV in the high-resolution XPS spectra were determined to be $2p_{3/2}$ and $2p_{1/2}$ states of Cu(I). The sulfur $2p_{3/2}$ and $2p_{1/2}$ peaks were identified at 161.8 and 162.6 eV, which agreed with the sulfides phase in the range of 160 and 164 eV. The tiny peaks at 232 and 229 eV were attributed to the Mo $3d_{3/2}$ and $3d_{5/2}$ orbitals, respectively, and were due to the small loading amount in the composite. The UV-Vis absorption spectra of Cu_2S nanoparticles, MoS_2/rGO hybrid, and Cu_2S-MoS_2/rGO composites are shown in Figure S2a. Compared with the spectrum of Cu_2S alone, the composite showed a much broader peak at the range of 300 to 400 nm, which originated from the strong absorption and interaction of MoS_2-rGO in this regime [24].

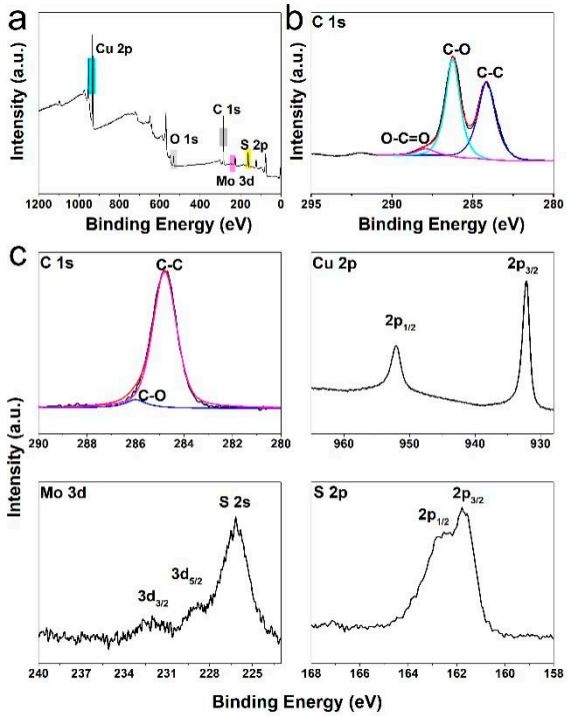

Figure 3. (**a**) Wide scan XPS spectrum and (**b**) high-resolution XPS spectrum in C 1s region of as-synthesized Cu_2S-MoS_2/rGO composite. (**c**) High-resolution XPS spectra for individual elements in Cu_2S-MoS_2/rGO composite, including C 1s, Cu 2p, Mo 3d, and S 2p.

Note that Cu_2S could be synthesized into several morphologies, but the simplest form of nanoparticles should work the best due to its copious number of active sites. To verify this, we first compared the photocatalytic hydrogen production rates of three types of Cu_2S nanocrystals, including nanoparticles, nanorods, and nanoplates. The preparation and characterization details of Cu_2S nanorods and nanoplates can be found in Figures S3 and S4, including TEM and XRD data. The photocatalytic hydrogen production rates of three types of Cu_2S nanocrystals are summarized in Figure 4a. The spherical Cu_2S nanoparticles showed the highest H_2 production rate of 234 μmol g^{-1} h^{-1}, compared with nanorods (123 μmol g^{-1} h^{-1}) and nanoplates (161 μmol g^{-1} h^{-1}). The small size (average 8.7 nm in diameter) of the nanoparticles resulted in a large surface area, which may provide more potential active sites for hydrogen evolution. The estimated band gap of 1.6 eV was significantly larger than bulk Cu_2S due to the quantum confinement effect, which may also decrease the chance of electron hole recombination, as shown in Figure S2b.

Cu_2S nanoparticles of the highest activity were selected for combining with co-catalyst MoS_2 and mediator rGO. The addition of 10 wt% rGO to Cu_2S nanoparticles showed a higher hydrogen generation rate of 260 μmol g^{-1} h^{-1}. An even higher photocatalytic activity can be achieved by loading 10 wt% MoS_2, resulting in a rate of 288 μmol g^{-1} h^{-1}. Compared to using rGO or MoS_2 as a single component, further enhancement was observed from the Cu_2S nanoparticles incorporated with MoS_2-rGO hybrid. The highest H_2 production rate (324 μmol g^{-1} h^{-1}) was obtained by the composites with the weight ratio of Cu_2S:MoS_2:rGO = 90:8.7:1.3. As a control experiment, Cu_2S nanoparticles and MoS_2-rGO hybrid were physically mixed with the ratio of Cu_2S:MoS_2:rGO = 90:8.7:1.3 in ethanol, sonicated for 2 h, and stirred overnight. The as-prepared physical mixture exhibited even lower photocatalytic activity than Cu_2S alone, as shown in Figure S5. Since the bare MoS_2/rGO hybrid showed a lower photocatalytic activity than Cu_2S, a simple physical mixing without forming interfacial contacts between Cu_2S and MoS_2/rGO hybrid did not enhance the photocatalytic activity. In summary, Cu_2S nanoparticles-decorated MoS_2-rGO hybrids exhibited the highest hydrogen generation rate of 324 μmol g^{-1} h^{-1}. The stability of Cu_2S-MoS_2/rGO composite was investigated by a continuous 9-h reaction

(Figure 4b). The produced amount of H_2 remained steady over the entire reaction time, indicating its excellent photocatalytic stability. The photocatalytic hydrogen production of Cu_2S-MoS_2/rGO composites was compared to those of previously reported relative photocatalysts, and are summarized in Table 1. The Cu_2S-MoS_2/rGO composites showed better hydrogen evolution performance than the Cu_2S/Pt and TiO_2/MoS_2/rGO system, even with lower light irradiation power.

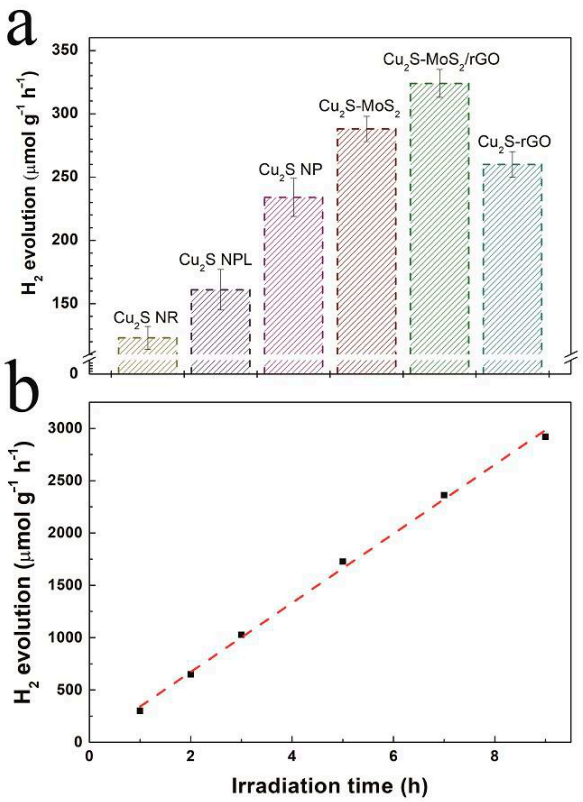

Figure 4. (**a**) Comparison of photocatalytic H_2 evolution from Cu_2S (Cu_2S nanorods: Cu_2S NR; Cu_2S nanoplates: Cu_2S NPL; Cu_2S nanoparticles: Cu_2S NP), Cu_2S-rGO, Cu_2S-MoS_2, and Cu_2S-MoS_2/rGO composites. Experimental conditions: 1-h irradiation by solar simulator (150 W Xe lamp, 100 mW cm^{-2}); (**b**) photocatalytic H_2 evolution by Cu_2S-MoS_2/rGO composites in a 9-h reaction. The composition of photocatalyst: 85 wt% Cu_2S, 13 wt% MoS_2, and 2 wt% rGO.

Table 1. Comparative photocatalytic hydrogen evolution with reference photocatalysts.

Photocatalyst	Light Source	Sacrificial Reagent	H_2 Production Rate ($\mu mol\ g^{-1}\ h^{-1}$)	Reference
Cu_2S-MoS_2/rGO	150 W Xenon	0.35M Na_2S/0.25M Na_2SO_3	324	This work
Au/MoS_2/rGO	300 W Xenon	0.25M methanol aq.	115.4	[29]
Cu_2S/Pt	300 W Xenon	0.1M Na_2S/0.5M Na_2SO_3	241.2	[30]
TiO_2/MoS_2/rGO	350 W Xenon	25% (*v*/*v*) ethanol/water	165.3	[27]
Cu_2ZnSnS_4/MoS_2/rGO	150 W Xenon	0.35M Na_2S/0.25M Na_2SO_3	104	[24]

A proposed mechanism for enhanced photocatalytic hydrogen evolution is illustrated in Scheme 1. Under the light irradiation, the electrons from the VB of Cu_2S were excited to the CB, leaving positively charged holes. The narrow bandgap enabled Cu_2S to efficiently absorb visible light, but it also make the excited electrons easily fall back to VB, resulting in electron-hole recombination, which lowered the photocatalytic activity. By the introduction of MoS_2 and rGO, the band structure of Cu_2S and MoS_2, as well as the Fermi level of rGO, allowed the photoexcited electrons to get transferred either directly to the CB of the nearby

MoS_2 or through rGO backbone to a remote MoS_2. The presence of rGO nanosheet with distinguished electron mobility served as an efficient electron collector [31]. Meanwhile, MoS_2 provided more active sites on the nanocrystal edges and fast electrochemical kinetics for hydrogen evolution reaction [32,33]. The dual-composite cocatalyst synergistically enhanced the photocatalytic hydrogen production of Cu_2S-MoS_2/rGO heterostructure. The photoexcited electrons on both Cu_2S and MoS_2 sulfur edges reacted with the adsorbed protons to produce H_2. Meanwhile, the holes were consumed by sacrificial agents, S^{2-} and SO_3^{2-}. Such electron transfer pathway suppressed the recombination of the electron-hole pairs, prolonged the lifetime of the excitons, provided more active sites for proton adsorption and hydrogen evolution, and consequently improved the photocatalytic hydrogen evolution rate.

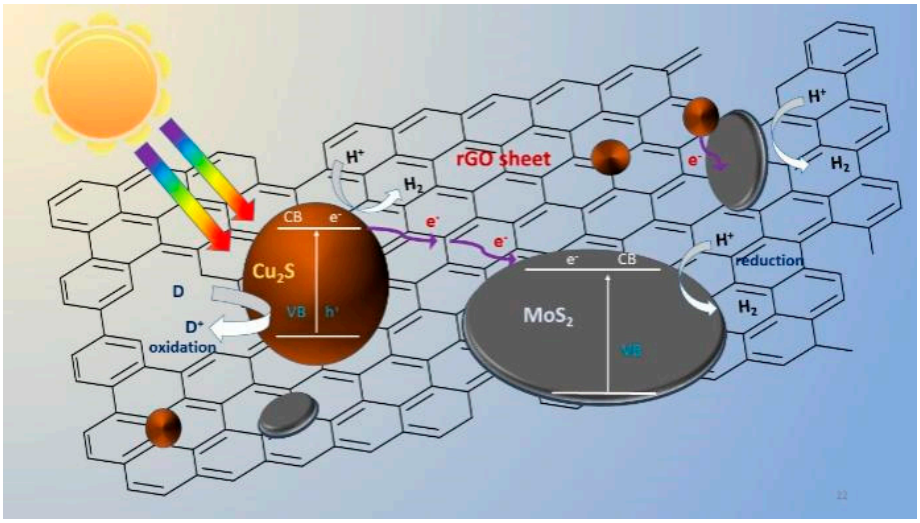

Scheme 1. Proposed mechanism of interfacial charge transfer and photocatalytic redox reaction in Cu_2S-MoS_2/rGO composites.

3. Experimental

3.1. Synthesis of Graphene Oxide (GO)

GO was prepared by an improved Hummer's method [34], which used strong oxidizing agents to chemically exfoliate the graphite sheet. Typically, 1 g graphite flakes were added to 150 mL (9:1 *v*/*v*) mixture of H_2SO_4/H_3PO_4, followed by slowly adding 6 g $KMnO_4$. After 36 h at room temperature, the mixture was poured into 200 mL ice with 3 mL H_2O_2 (30%). Then the mixture was centrifuged and washed in succession with DI water until the pH of the supernatant was between 4~5. The solid was further purified by dialysis using Wizard® SVmini columns (A129B) for 1 week. After the purification steps, the mixture was then under ultrasonication for 1 h, centrifugation, and air drying for the supernatant. This procedure was repeated for the remaining precipitates.

3.2. Synthesis of 1T-MoS_2/rGO Hybrid

The 1T-MoS_2 and 1T-MoS_2/rGO hybrid were prepared through a hydrothermal method [25]. Sodium molybdate dehydrates ($Na_2MoO_4 \cdot 2H_2O$) and thiourea ($CS(NH_2)_2$) were chosen as Mo precursor and S precursor, respectively. For the synthesis of 1T-MoS_2/rGO hybrid, 0.242 g $Na_2MoO_4 \cdot 2H_2O$, 2.28 g $CS(NH_2)_2$, and a certain amount of GO was dispersed into 30 mL DI water by the assistance of ultrasonication for 20 min. The pH value was adjusted to 6.5 by NaOH solution. Then the mixture was transferred to a 45-mL Teflon-lined stainless steel autoclave, maintained at 200 °C for 24 h, and allowed naturally to cool down to room temperature. The product was washed with ethanol several times and vacuum dried at 60 °C.

3.3. Synthesis of Cu_2S Nanostructures and Cu_2S-MoS_2/rGO Composites

The nanoparticles, nanorods, and nanoplates of Cu_2S were synthesized through a hot injection method, reported previously by Yue Wu et al. [16], Marta Kruszynska et al. [12], and Yan Wang et al. [16], respectively. In a typical synthesis of Cu_2S nanoparticles, 281.6 mg ammonium diethyldithiocarbamate and 10 mL 1-dodecanethiol (1-DDT) were mixed with 17 mL oleic acid. After the purging process, the reaction solution was heated up to 110 °C under N_2 protection, and a suspension of 261.8 mg copper (II) acetylacetonate [$Cu(acac)_2$] and 3 mL oleic acid was injected into the system. Then the temperature was raised to 180 °C and kept for 10 min. The resulting product was cooled to room temperature, washed with chloroform and ethanol at least three times, and dried in a vacuum oven. The following Cu_2S nanostructures were also purified in this way.

In the preparation of Cu_2S nanoplates, 181.6 mg copper (II) acetate and 2.5 g trioctylphosphine oxide (TOPO) were dissolved in 30 mL 1-octadecene (ODE) in a three-neck flask. The mixture was stirred under vacuum for 1 h followed by bubbling with nitrogen gas (N_2) to remove any low-boiling-point solvents. Thereafter, the reaction solution was heated up to 160 °C under N_2 flow followed by a quick injection of 2.5 mL 1-DDT. Then the temperature was raised to 200 °C and kept for 1.5 h. The resulting product was cooled to room temperature, washed with chloroform and ethanol at least three times, and dried in a vacuum oven. After the reaction, the resulting product was separated, cleaned, and dried.

To obtain Cu_2S nanorods, the replacement of 1-DDT by *tert*-dodecanethiol (*t*-DDT) was required. Then, 181.6 mg copper (II) acetate and 1.9 g TOPO were dissolved in 10 mL ODE, and the mixture was purged in the same manner. Under N_2 flow, 3.75 mL of *t*-DDT was injected into the system when the reaction solution was heated to 120 °C. Then, the temperature was raised to 180 °C. The reaction was allowed to proceed for 3–5 min, and the product was then cooled, purified, and dried.

For the synthesis of Cu_2S-MoS_2/rGO composites, a certain amount of MoS_2/rGO was dispersed into sulfur precursor solution by 30-min sonication and reacted with a metal precursor.

3.4. Characterization and Photocatalytic Test

The crystalline structure of the nanostructures was characterized by powder X-ray diffraction (PXRD), which was performed on a SmartLab® X-ray diffractometer (Rigaku, Tokyo, Japan) at room temperature with Cu Kα radiation (λ = 1.5418 Å) and a diffraction angle 2θ ranging from 5° to 90°. The structural and morphological information was obtained by using a JEM-2100F (JEOL Ltd., Tokyo, Japan) scanning transmission electron microscope (STEM) and selected area electron diffraction (SAED) operated at 200-kV accelerating voltage. The analysis of elemental compositions was conducted on an energy dispersive X-ray spectrometer (EDS) attached to the STEM. For TEM and EDS measurements, samples were dispersed in chloroform by sonication and drop-dried on holey carbon-coated 400-mesh Ni grids. UV-Visible absorption spectra were recorded on an Agilent 8453 Diode-Array UV-Visible spectrophotometer (Santa Clara, CA, USA) within the wavelength range of 200~1000 nm. Before the measurement, samples were dispersed in chloroform in a quartz cuvette of 1-cm path length. The XPS results were obtained by the instrument of Thermo Fisher Scientific K-Alpha (Waltham, MA, USA).

For the measurement of photocatalytic hydrogen evolution, light irradiation was performed at ambient temperature and atmospheric pressure with a Newport solar simulator (Xenon lamp, ozone free, 150 W) (Irvine, CA, USA) of light intensity of 100 mW cm^{-2} for 3 h. In a typical photocatalytic experiment, the catalyst of ca. 5 mg was dispersed by 10-min sonication in 25 mL aqueous sulfide/sulfite solution (0.35M Na_2S/0.25M Na_2SO_3). Prior to irradiation, Argon was bubbled through the reactor for 30 min to achieve anaerobic conditions. The solution was stirred throughout the irradiation period in order to keep the photocatalyst in suspension status. After irradiation, 250 µL gas was injected and analyzed by Agilent 7890B gas chromatograph system (Palo Alto, CA, USA) (TCD, nitrogen as carrier gas).

4. Conclusions

In this work, a novel Cu_2S-based composite photocatalyst containing MoS_2/rGO hybrid as a cocatalyst was synthesized and characterized. The study of the morphology effect of Cu_2S nanocrystals showed that the Cu_2S nanoparticles with chalcocite structure had a higher photocatalytic hydrogen production rate (234 μmol g^{-1} h^{-1}) compared with Cu_2S nanoplates (chalcocite, 161 μmol g^{-1} h^{-1}) and Cu_2S nano-rods (djurleite, 123 μmol g^{-1} h^{-1}). The Cu_2S-MoS_2/rGO composites with a ratio of Cu_2S:MoS_2:rGO = 90:8.7:1.3 showed the highest photocatalytic hydrogen production rate of 324 μmol g^{-1} h^{-1}. It is believed that the synergistic effect between the photocatalyst Cu_2S and cocatalyst/mediator MoS_2/rGO hybrid can effectively isolate photoexcited electrons and reduce the recombination of the electron-hole pairs, thus enhancing the photocatalytic hydrogen evolution performance.

Supplementary Materials: The following are available online at https://www.mdpi.com/article/10.3390/catal11111278/s1. Figure S1: EDS spectrum of Cu_2S-MoS_2/rGO composites. Figure S2: (a) UV-Vis spectra of Cu_2S-MoS_2/rGO, MoS_2/rGO, and Cu_2S; (b) the band gap calculation of Cu_2S by using Tauc plot. Figure S3: Typical TEM images of (a) Cu_2S nanoparticles, (c) nanorods, (e) nanoplates and their corresponding size distribution histograms (b, d, f). Figure S4: Powder XRD patterns of as-synthesized Cu_2S nanoparticles, nanoplates, and nanorods. Figure S5: H_2 generation from various Cu_2S-MoS_2/rGO composites with different ratios compared to their physical mixture.

Author Contributions: Conceptualization, E.H. and J.H.; methodology, Z.X.; formal analysis, Z.X.; data curation, D.L. and J.Z.; writing—original draft preparation, E.H. and Z.X.; writing—review and editing, T.J. and X.H.; supervision, L.W. and J.H.; funding acquisition, E.H. and J.H. All authors have read and agreed to the published version of the manuscript.

Funding: This research was funded by the Natural Science Foundation of Top Talent of SZTU (Grant No. 2019205), National Natural Science Foundation of China (Grant Nos. 21701135, 21902104, and 21561031), Shenzhen Science and Technology Research Project (Grant No. JCYJ20170818093553012), the Open Project Program of Key Laboratory for Analytical Science of Food Safety and Biology, Ministry of Education (Grant No. FS2004), Foundation for Young Innovative Talents in Higher Education of Guangdong (Grant No. 2018KQNCX401), and the Guangdong Basic and Applied Basic Research Foundation (Grant No. 2020A1515010258).

Acknowledgments: The authors would like to thank the helpful discussion and support from Lawrence Yoon Suk Lee and Kwok-Yin Wong at the Hong Kong Polytechnic University, Hong Kong SAR.

Conflicts of Interest: The authors declare no conflict of interest.

References

1. Liu, M.; Liu, Y.; Gu, B.; Wei, X.; Xu, G.; Wang, X.; Swihart, M.T.; Yong, K.-T. Recent advances in copper sulphide-based nanoheterostructures. *Chem. Soc. Rev.* **2019**, *48*, 4950–4965. [CrossRef]
2. Nikam, A.N.; Pandey, A.; Fernandes, G.; Kulkarni, S.; Mutalik, S.P.; Padya, B.S.; George, S.D.; Mutalik, S. Copper sulphide based heterogeneous nanoplatforms for multimodal therapy and imaging of cancer: Recent advances and toxicological perspectives. *Coord. Chem. Rev.* **2020**, *419*, 213356. [CrossRef]
3. Cui, J.; Jiang, R.; Guo, C.; Bai, X.; Xu, S.; Wang, L. Fluorine Grafted Cu_7S_4–Au Heterodimers for Multimodal Imaging Guided Photothermal Therapy with High Penetration Depth. *J. Am. Chem. Soc.* **2018**, *140*, 5890–5894. [CrossRef]
4. Peng, Q.K.; Zhang, S.P.; Yang, H.; Sheng, B.B.; Xu, R.; Wang, Q.S.; Yu, Y. Boosting Potassium Storage Performance of the Cu_2S Anode via Morphology Engineering and Electrolyte Chemistry. *ACS Nano* **2020**, *14*, 6024–6033. [CrossRef] [PubMed]
5. Chen, X.; Xu, W.; Ding, N.; Ji, Y.; Pan, G.; Zhu, J.; Zhou, D.; Wu, Y.; Chen, C.; Song, H. Dual Interfacial Modification Engineering with 2D MXene Quantum Dots and Copper Sulphide Nanocrystals Enabled High-Performance Perovskite Solar Cells. *Adv. Funct. Mater.* **2020**, *30*, 2003295. [CrossRef]
6. Srinivas, B.; Kumar, B.G.; Muralidharan, K. Stabilizer free copper sulphide nanostructures for rapid photocatalytic decomposition of rhodamine B. *J. Mol. Catal. A Chem.* **2015**, *410*, 8–18. [CrossRef]
7. Zhuang, Z.; Peng, Q.; Zhang, B.; Li, Y. Controllable Synthesis of Cu_2S Nanocrystals and Their Assembly into a Superlattice. *J. Am. Chem. Soc.* **2008**, *130*, 10482–10483. [CrossRef]
8. Xie, Y.; Riedinger, A.; Prato, M.; Casu, A.; Genovese, A.; Guardia, P.; Sottini, S.; Sangregorio, C.; Miszta, K.; Ghosh, S.; et al. Copper Sulfide Nanocrystals with Tunable Composition by Reduction of Covellite Nanocrystals with Cu^+ Ions. *J. Am. Chem. Soc.* **2013**, *135*, 17630–17637. [CrossRef]

9. Wu, Y.; Wadia, C.; Ma, W.; Sadtler, B.; Alivisatos, A.P. Synthesis and Photovoltaic Application of Copper(I) Sulfide Nanocrystals. *Nano Lett.* **2008**, *8*, 2551–2555. [CrossRef]
10. Liu, Z.; Xu, D.; Liang, J.; Shen, J.; Zhang, S.; Qian, Y. Growth of Cu_2S Ultrathin Nanowires in a Binary Surfactant Solvent. *J. Phys. Chem. B* **2005**, *109*, 10699–10704. [CrossRef]
11. Law, M.; Greene, L.E.; Johnson, J.C.; Saykally, R.; Yang, P. Nanowire dye-sensitized solar cells. *Nat. Mater.* **2005**, *4*, 455–459. [CrossRef]
12. Kruszynska, M.; Borchert, H.; Bachmatiuk, A.; Rümmeli, M.H.; Büchner, B.; Parisi, J.; Kolny-Olesiak, J. Size and Shape Control of Colloidal Copper(I) Sulfide Nanorods. *ACS Nano* **2012**, *6*, 5889–5896. [CrossRef] [PubMed]
13. Sigman, M.B.; Ghezelbash, A.; Hanrath, T.; Saunders, A.E.; Lee, F.; Korgel, B.A. Solventless Synthesis of Monodisperse Cu_2S Nanorods, Nanodisks, and Nanoplatelets. *J. Am. Chem. Soc.* **2003**, *125*, 16050–16057. [CrossRef] [PubMed]
14. Hui, Z.; Xu, W.; Li, X.; Guo, P.; Zhang, Y.; Liu, J. Cu_2S nanosheets for ultrashort pulse generation in the near-infrared region. *Nanoscale* **2019**, *11*, 6045–6051. [CrossRef] [PubMed]
15. Li, X.; Shen, H.; Niu, J.; Li, S.; Zhang, Y.; Wang, H.; Li, L.S. Columnar Self-Assembly of Cu_2S Hexagonal Nanoplates Induced by Tin(IV)−X Complex as Inorganic Surface Ligand. *J. Am. Chem. Soc.* **2010**, *132*, 12778–12779. [CrossRef] [PubMed]
16. Wang, Y.; Hu, Y.; Zhang, Q.; Ge, J.; Lu, Z.; Hou, Y.; Yin, Y. One-Pot Synthesis and Optical Property of Copper(I) Sulfide Nanodisks. *Inorg. Chem.* **2010**, *49*, 6601–6608. [CrossRef] [PubMed]
17. Liu, G.; Schulmeyer, T.; Brötz, J.; Klein, A.; Jaegermann, W. Interface properties and band alignment of Cu_2S/CdS thin film solar cells. *Thin Solid Films* **2003**, *431-432*, 477–482. [CrossRef]
18. Marschall, R. Semiconductor Composites: Strategies for Enhancing Charge Carrier Separation to Improve Photocatalytic Activity. *Adv. Funct. Mater.* **2014**, *24*, 2421–2440. [CrossRef]
19. Zhu, J.; Hu, L.; Zhao, P.; Lee, L.Y.S.; Wong, K.-Y. Recent Advances in Electrocatalytic Hydrogen Evolution Using Nanoparticles. *Chem. Rev.* **2020**, *120*, 851–918. [CrossRef]
20. Lin, H.; Zhang, K.; Yang, G.; Li, Y.; Liu, X.; Chang, K.; Xuan, Y.; Ye, J. Ultrafine nano 1T-MoS_2 monolayers with NiO_x as dual co-catalysts over TiO_2 photoharvester for efficient photocatalytic hydrogen evolution. *Appl. Catal. B Environ.* **2020**, *279*, 119387. [CrossRef]
21. Wang, Y.; Lu, F.; Su, K.; Zhang, N.; Zhang, Y.; Wang, M.; Wang, X. Engineering Mo-O-C interface in MoS_2@rGO via charge transfer boosts hydrogen evolution. *Chem. Eng. J.* **2020**, *399*, 126018. [CrossRef]
22. Zhang, X.; Guo, Y.; Tian, J.; Sun, B.; Liang, Z.; Xu, X.; Cui, H. Controllable growth of MoS_2 nanosheets on novel Cu_2S snowflakes with high photocatalytic activity. *Appl. Catal. B Environ.* **2018**, *232*, 355–364. [CrossRef]
23. Liu, L.; Liu, X.; Jiao, S. CuS@defect-rich MoS_2 core-shell structure for enhanced hydrogen evolution. *J. Colloid Interface Sci.* **2020**, *564*, 77–87. [CrossRef]
24. Ha, E.; Liu, W.; Wang, L.; Man, H.-W.; Hu, L.; Tsang, S.C.E.; Chan, C.T.-L.; Kwok, W.-M.; Lee, L.Y.S.; Wong, K.-Y. Cu_2ZnSnS_4/MoS_2-Reduced Graphene Oxide Heterostructure: Nanoscale Interfacial Contact and Enhanced Photocatalytic Hydrogen Generation. *Sci. Rep.* **2017**, *7*, 39411. [CrossRef]
25. Liu, Q.; Li, X.; He, Q.; Khalil, A.; Liu, D.; Xiang, T.; Wu, X.; Song, L. Gram-Scale Aqueous Synthesis of Stable Few-Layered 1T-MoS_2: Applications for Visible-Light-Driven Photocatalytic Hydrogen Evolution. *Small* **2015**, *11*, 5556–5564. [CrossRef]
26. Zhu, B.; Lin, B.; Zhou, Y.; Sun, P.; Yao, Q.; Chen, Y.; Gao, B. Enhanced photocatalytic H_2 evolution on ZnS loaded with graphene and MoS_2 nanosheets as cocatalysts. *J. Mater. Chem. A* **2014**, *2*, 3819–3827. [CrossRef]
27. Xiang, Q.; Yu, J.; Jaroniec, M. Synergetic Effect of MoS_2 and Graphene as Cocatalysts for Enhanced Photocatalytic H_2 Production Activity of TiO_2 Nanoparticles. *J. Am. Chem. Soc.* **2012**, *134*, 6575–6578. [CrossRef] [PubMed]
28. Wang, L.; Lian, J.; Cui, P.; Xu, Y.; Seo, S.; Lee, J.; Chan, Y.; Lee, H. Dual n-type doped reduced graphene oxide field effect transistors controlled by semiconductor nanocrystals. *Chem. Commun.* **2012**, *48*, 4052–4054. [CrossRef] [PubMed]
29. Yu, X.; Shi, J.; Wang, L.; Wang, W.; Bian, J.; Feng, L.; Li, C. A novel Au NPs-loaded MoS_2/RGO composite for efficient hydrogen evolution under visible light. *Mater. Lett.* **2016**, *182*, 125–128. [CrossRef]
30. Wang, B.; An, W.; Liu, L.; Chen, W.; Liang, Y.; Cui, W. Novel Cu_2S quantum dots coupled flower-like BiOBr for efficient photocatalytic hydrogen production under visible light. *RSC Adv.* **2015**, *5*, 3224–3231. [CrossRef]
31. Geim, A.K.; Novoselov, K.S. The rise of graphene. *Nat. Mater.* **2007**, *6*, 183–191. [CrossRef] [PubMed]
32. Jaramillo, T.F.; Jørgensen, K.P.; Bonde, J.; Nielsen, J.H.; Horch, S.; Chorkendorff, I. Identification of Active Edge Sites for Electrochemical H_2 Evolution from MoS_2 Nanocatalysts. *Science* **2007**, *317*, 100–102. [CrossRef] [PubMed]
33. Wang, X.; Long, R. Rapid Charge Separation Boosts Solar Hydrogen Generation at the Graphene–MoS_2 Junction: Time-Domain Ab Initio Analysis. *J. Phys. Chem. Lett.* **2021**, *12*, 2763–2769. [CrossRef] [PubMed]
34. Marcano, D.C.; Kosynkin, D.V.; Berlin, J.M.; Sinitskii, A.; Sun, Z.; Slesarev, A.; Alemany, L.B.; Lu, W.; Tour, J.M. Improved Synthesis of Graphene Oxide. *ACS Nano* **2010**, *4*, 4806–4814. [CrossRef]